INVESTIGATION OF LOAD TRANSFER BETWEEN THE FIBER AND THE MATRIX IN PULL-OUT TESTS WITH FIBERS HAVING DIFFERENT DIAMETERS

S. Zhandarov[1], E. Pisanova[1], E. Mäder[1], and J. A. Nairn*, [2]

1. Institute of Polymer Research Dresden e.V.,

Hohe Str. 6, Dresden 01069, Germany

2. Materials Science and Engineering Department

University of Utah, Salt Lake City, UT 84112, USA

Running head: Pull-out tests with fibers having different diameters

* To whom correspondence should be addressed.

Corresponding author:
PROF. JOHN A. NAIRN
DEPT. OF MATERIALS SCIENCE & ENGINEERING
UNIVERSITY OF UTAH
122 S CENTRAL CAMPUS DR RM 304
SALT LAKE CITY UT 84112
USA
Phone: +1-801-581-3413
Fax: +1-801-581-4816
E-mail: John.Nairn@m.cc.utah.edu

ABSTRACT

Single-fiber pull-out tests were used for investigation of interfacial bond strength or toughness and load transfer between polymeric matrices and glass fibers having different diameters. The interfacial bond strength was well characterized by an ultimate interfacial shear strength (τ_{ult}) whose values were nearly independent of fiber diameter. The same experiments were also analyzed by fracture mechanics methods to determine the interfacial toughness (G_{ic}). The critical energy release rate (G_{ic}) was a good material property for constant fiber diameter, but G_{ic} for initiation of debonding typically got smaller as the fiber diameter got larger. It was also possible to measure an effective shear-lag parameter, β, characterizing load transfer efficiency between the fiber and the matrix. β decreased considerably with the fiber radius; this decrease scaled roughly as expected from elasticity theory. The measured results for β were used to calculate the radius of matrix material surrounding the fiber and significantly affected by the presence of the fiber. The ratio of this radius to the fiber radius (R_m/r_f) was a function of fiber diameter.

Keywords: pull-out test; load transfer; ultimate interfacial shear strength; critical energy release rate; shear-lag parameter.

1. INTRODUCTION

The efficiency of load transfer through the interface between the fiber and the matrix plays a critical role in the performance and behavior of fiber-reinforced composite materials. To investigate this efficiency, a number of micromechanical techniques, such as pull-out, push-out, microbond, and fragmentation tests, have been extensively used in recent decades [1–4]. These tests have been considered to be convenient for estimation of the efficiency of fiber surface treatments, matrix modification, *etc*. The results, however, from different tests, or even from the same test but obtained by different researchers, are hardly comparable [4]. This difference is mostly due to inadequate experimental data reduction methods. For example, specimen geometry can greatly affect the load transfer but it is often ignored or mistreated.

Traditionally, load transfer through the interface has been characterized by an apparent interfacial shear strength (τ_{app}). τ_{app}, however, is only an effective (mean) value which depends on many factors, such as embedded fiber length and interfacial friction between the matrix and the debonded fiber. In more recent work, local interfacial parameters, such as ultimate (local, critical) interfacial shear strength (τ_{ult}) [5–9] and critical energy release rate (G_{ic}) [10–12], are being used for interface characterization in fiber-matrix systems. The important advantage of these parameters is that they are regarded as true failure criteria, in other words, they characterize local processes near crack tips that lead to interfacial debonding.

To estimate τ_{ult} and G_{ic} from experimental results requires the use of an elasticity model. The most popular elastic models are one-dimensional shear-lag models by Cox [13] and Nayfeh [14] and a three-dimensional model proposed by Scheer and Nairn [10]. An important parameter in these models is the matrix volume effectively involved in load transfer, or, in other words, the "external radius" of the matrix relative to the fiber radius. In multi-fiber, unidirectional

composites, this volume fraction is often assumed to be the distance between neighboring fibers. For single-fiber micromechanical tests, however, the meaning of "matrix radius" is rather blurred. A typical micromechanical sample is a single fiber having a diameter of several micrometers embedded in a droplet or bar of matrix material with a much larger transverse size (several millimeters). Matrix droplets, such as in microbond tests, however, differ in their size depending on droplet length [10]. It is, therefore, not surprising that different researchers obtain different results even when using the same equations for the same fiber-matrix materials pair. Most microbond analyses have not even included droplet diameter in the analysis, but it has recently been shown that the failure load depends on droplet diameter and thus this term must be included to obtain valid results [10, 11]. Furthermore, in test methods that typically use much more matrix material than microbond tests, it is likely that only a small part of the matrix volume is involved in load transfer. The participation of only a thin layer of matrix adjacent to the fiber was shown experimentally using birefringence techniques [15] and Raman spectroscopy [16]. Using the latter technique, Andrews et al. [17] estimated the effective ratio R_m/r_f (where R_m and r_f are the effectively loaded radius of the matrix and the radius of the fiber, respectively) for aramid–epoxy systems (aramid fibers having diameter of $r_f = 12\,\mu\text{m}$) to be about $R_m/r_f = 15$. Other measurements and theoretical estimations [18, 19] suggest that a value of R_m/r_f in the range of 2 to 10 is typical for high-modulus fibers in a polymeric matrix. It is not clear whether this estimation is valid for all polymer-fiber systems, or, even whether it is the same for a single polymer-fiber pair but with fibers of different radii.

Clearly R_m/r_f will decrease as the fiber radius increases when R_m is constant. Further study on this issue could provide important information for better comparisons between micromechanical tests using different fiber diameters and between different micromechanical tests. In this study, single-fiber pull-out tests were done on a series of glass fibers having different diameters and

different sizings in a variety of polymeric matrices. The simultaneous analysis of all results led to better characterization of the efficiency of load transfer between glass fibers and polymer matrices.

2. EXPERIMENTAL

2.1. Materials

E-glass fibers manufactured using spinning devices at the Institute of Polymer Research Dresden were used in these experiments. The fiber diameters varied from 9 to 90 μm. Several sizings and/or coatings were used in order to modify the surface of the glass fibers and to alter the bond strengths between them and polymer matrices. The unsized fibers are designated in this paper as G0, and the treated fibers are designated G1 (γ-aminopropyltriethyoxysilane sizing, γ-APS), G2 (γ-APS sizing with polyurethane film former), G3 (polyvinyl alcohol coating) and G4 (methacryltriethoxysilane sizing + unsaturated polyester film former).

For matrix materials, we used three thermoplastic polymers and one thermoset polymer. The thermoplastic polymers used were polyamide 6 (PA6, Leuna Werke AG), polyamide 6,6 (PA66, Ultramid A5, BASF) and maleic anhydride grafted polypropylene (PPM). The last was produced by blending the commercial modifier M1 with polypropylene homopolymer from Borealis in an amount of 2 wt% during compounding in a twin-screw extruder. The thermoset polymer used was vinylester resin (VE) manufactured by Norpol.

The mechanical properties of fibers and matrices, necessary for interfacial bond strength and toughness characterization, are given in Table 1.

2.2. Pull-Out Tests

The pull-out tests were carried out using a pull-out apparatus which allows high precision fiber displacement and force measurements as well as data recording and management [20]. The

fibers were embedded in thermoplastic matrices in a microwave oven under argon atmosphere. The heating and cooling rates were about 50°C/min. For the thermosetting VE resin, the specimens were cured after embedding the fiber at 70°C for 1 h. The embedded lengths ranged from 50 to300 μm.

All pull-out tests were performed at a constant crosshead displacement rate of 1.2×10^{-2} mm/min for all specimens and tested at ambient temperature. Force-displacement curves were recorded. From each force-displacement curve, the debond force, F_d (which corresponds to interfacial crack initiation and manifests itself as a deviation from linearity or a "kink" in the growing stage of the curve, see Fig. 1), and the embedded fiber length, l_e, were determined. The apparent or debond shear stress, τ_d, was calculated using

$$\tau_d = F_d / \left(2\pi r_f l_e\right). \tag{1}$$

The interfacial strength and interfacial toughness were characterized using three parameters, as described in Section 3.

3. THEORY

3.1. Shear-lag parameter and its relation to an "effectively loaded matrix radius"

Finding the exact stress distribution in a specimen consisting of an elastic cylindrical fiber that is being pulled out of an elastic matrix is a complicated task. Even when using a simple geometry (*e.g.*, a cylindrical matrix surrounding the fiber), further simplifying assumptions are required in order to obtain analytical results.

Several simplified approaches that describe interfacial stress distribution along the embedded fiber length are known. One-dimensional shear-lag models [8, 13, 21] are commonly used. From such shear-lag analyses, it is possible to obtain the interfacial shear stress as a function of a

coordinate along the fiber. In shear-lag analysis, the maximum interfacial shear stress occurs where the fiber enters the matrix. If one assumes debonding occurs when this maximum interfacial shear stresses reaches τ_{ult}, or the critical (ultimate) interfacial shear strength, then it is possible to predict that the debond force, F_d (external load at which interfacial debonding initiates) is given by [22]:

$$F_d = \frac{2\pi r_f \tau_{ult}}{\beta} \tanh \beta l_e - \pi r_f^2 \sigma_T \tanh \beta l_e \tanh \frac{\beta l_e}{2}, \qquad (2)$$

where l_e is the embedded fiber length, r_f is the fiber radius, σ_T is the magnitude of the radial compressive stress resulting from thermal shrinkage of the fiber and the matrix [23, 25], and β is the shear-lag parameter. Equation (2) can also be written in terms of the apparent debond shear stress, τ_d (see Eq. (1)) as:

$$\tau_d = \left(\tau_{ult} - \frac{\beta r_f}{2} \sigma_T \tanh \frac{\beta l_e}{2} \right) \frac{\tanh \beta l_e}{\beta l_e}. \qquad (3)$$

It is important that neither Eq. (2) nor Eq. (3) require any particular expression for β, and thus β can be considered as a fitting parameter to be determined from experimental data if it is assumed that β and τ_{ult} are constants for a given set of experiments. Note that τ_d is different from the commonly used apparent interfacial shear strength (τ_{app}). τ_{app} is usually calculated using the maximum applied load, F_{max}, and corresponds to the *average* shear stress on the interface at the peak load. Here, τ_d was calculated from the force at the onset of debonding, F_d, and it corresponds to the *average* shear stress on the interface at this lower load.

For a quantitative characterization of load transfer through the interface and of interfacial bond strength, the procedure described in [8] was used. The experimental τ_d values were plotted against embedded lengths using Eq. (3). The best fit between experiments and Eq. (3), with β and

τ_{ult} as fitting parameters, was found using the least-squares method. For the low-fiber volume fractions present in single-fiber pull-out tests, the thermal stress term, σ_T, can be calculated with sufficient accuracy using

$$\sigma_T = E_f(\alpha_A - \alpha_m)\Delta T \tag{4}$$

where E_f is the (axial) tensile modulus of the fiber, α_A is the axial thermal expansion coefficient of the fiber, α_m is the thermal expansion coefficient of the matrix, and ΔT is the temperature difference between the test temperature and the stress-free temperature (see Table 1). The optimum τ_{ult} value from the above fitting procedure was considered to be the ultimate interfacial shear strength for the given polymer-fiber-sizing specimens [8, 24].

The optimum β was considered to be a *measured* stress-transfer parameter that characterizes the distribution of interfacial shear stresses in the specimen (*i.e.*, the key parameter in a shear-lag stress analysis). Although β here is a *measured* quantity, in shear-lag theories of stress transfer, β is a parameter that is *calculated* from specimen geometry and mechanical properties of the fiber and the matrix [25]. There are two explicit expressions for finding β from fiber, matrix, and specimen properties. In the original Cox approach [13], the shear-lag parameter is defined by

$$\beta = \left(\frac{2G_m}{E_f r_f^2 \ln \frac{R_m}{r_f}} \right)^{1/2} \tag{5}$$

where G_m is the matrix shear modulus and R_m is the "effectively-loaded matrix radius".

Despite the popularity of the Cox analysis and the Cox shear-lag parameter, it has recently been shown that it never gives a valid calculation of stress transfer in concentric cylinder model

calculations [11, 25]. Instead, in all fiber/matrix shear-lag analyses, the Cox shear-lag parameter should be replaced by the shear-lag parameter originally derived by Nayfeh [14] and given by:

$$\beta = \left\{ \frac{2}{r_f^2 E_f E_m} \left[\frac{E_f V_f + E_m V_m}{\frac{V_m}{4G_f} + \frac{1}{2G_m}\left(\frac{1}{V_m} \ln \frac{1}{V_f} - 1 - \frac{V_f}{2} \right)} \right] \right\}^{1/2} \qquad (6)$$

where E_m is Young's modulus of the matrix, G_f is the (axial) shear modulus of the fiber, and V_f and V_m are the volume fractions of the fiber and the matrix, respectively. When the matrix is approximated by a cylinder, the fiber volume fraction is $V_f = (r_f/R_m)^2$ and $V_m = 1 - V_f$.

Again, given fiber, matrix, and specimen properties, Eqs. (5) and (6) give two results for calculating the shear-lag stress-transfer parameter β. Here a different approach was taken. The experiments provided a method for measuring β. Given fiber and matrix properties and a measured result for β, Eqs. (5) and (6) can be inverted to determine the effectively-loaded matrix radius, R_m. Thus, in contrast to common approaches, which either consider R_m as the radius of the specimen (matrix droplet) or take a "reasonable" but arbitrary value for the R_m/r_f ratio, given an experimental β value, Eqs. (5) and (6) allow calculation of R_m. Note that both Eq. (5) and (6) predict that β approaches zero as R_m approaches infinity. In other words shear-lag analysis breaks down at low fiber volume fractions. To use shear-lag analysis for very low fiber volume fractions, the true fiber volume fraction must always be replaced by a volume fraction deduced from the effectively-loaded matrix radius which is deduced here from the measured β. Because Eq. (5) is never correct at any volume fraction [25], only Eq. (6) will give an estimation of an effectively-loaded matrix radius that corresponds to the actual radius within the matrix where the stresses are significantly perturbed by the presence of the fiber.

3.2. Interfacial fracture toughness

The quality of bonding at fiber-matrix interfaces can be characterized by either local (ultimate) interfacial shear stress (IFSS or τ_{ult}) [5–9] or by a critical energy release rate for interfacial crack propagation (G_{ic}) [10–12]. During the last two decades, the question of which of them describes the interface "better" has been extensively discussed in the literature. Many papers have been published in support of each, referring mainly to different theoretical models for micromechanical tests. This discussion is closely related to the problem of the proper choice of failure criterion: is it stress-based or energy-based? The failure criterion, in turn, depends on the mechanism of interfacial failure, which cannot be predicted *a priori* by theoretical or numerical models, but rather requires experimental investigations.

The analysis of experimental data showed that both τ_{ult} and G_{ic} were good candidates for the failure criteria. They each adequately describe interfacial crack propagation [23] and can predict debond force in the pull-out or microbond tests as a function of embedded fiber length [22]. Moreover, it was demonstrated that for specimens containing fibers of the same diameter these two parameters could be used as essentially equivalent failure criteria [22, 23]. τ_{ult} and G_{ic}, however, may depend on fiber diameter. Several possible trends for their variation with r_f have been considered theoretically [22]. Unfortunately, data from micromechanical tests on fibers with different diameters are very scarce. One goal of this study was to estimate the values of interfacial parameters for polymer/glass-fiber systems with glass fibers having the same chemical structure but differing diameters. These results can be used to evaluate the τ_{ult} and G_{ic} failure criteria. Clearly, a true failure criterion should be a constant for a given pair of materials and independent of specimen geometry.

The ultimate interfacial shear strength was calculated by fitting experimental results to Eq. (3). To estimate G_{ic}, the model developed by Scheer and Nairn [10] and Liu and Nairn [11] was used. That model, however, was developed for the microbond test. It has recently been extended to handle the pull-out test as well [26]. For initiation of debonding (initial debond length equal to zero), frictionless debonding, and sufficiently long embedded fiber lengths, the critical energy release rate is given by [26]:

$$G_{ic} = \frac{r_f}{2}\left[C_{33s}\sigma_r^2 + 2D_{3s}\sigma_r\Delta T + \left(\frac{D_3^2}{C_{33}} + \frac{V_m(\alpha_T - \alpha_m)^2}{V_f A_0} \right)(\Delta T)^2 \right]. \qquad (7)$$

where $\sigma_r = F_d\, E_m\, V_m/(\pi\, r_f^2\, E_c)$ is a reduced stress applied to the fiber at the moment of crack initiation, $E_c = E_f V_f + E_m V_m$ is the rule-of-mixture modulus of the specimen, α_T is the transverse thermal expansion coefficient of the fiber, and C_{33}, D_{3s}, D_3, C_{33s}, and A_0 are constants defined in the *Appendix* which depend only on fiber and matrix properties and on specimen geometry [10, 26]. The analysis in Ref. [26] also considers frictional stress on debond surfaces and the effects of short embedded fiber lengths. Some sample calculations showed that both these effects could be ignored for analysis of our experimental results. Friction could be ignored because we only analyzed *initiation* of debonding. Although friction affects G_{ic} for initiation [26], it had to be much higher than reasonably thought possible to have a significant effect on the results. Similarly, a comparison of analyses that assume long embedded fibers with those that account for short fiber lengths [26] showed that the long-fiber analysis was adequate. There were some deviations for the shortest embedded fiber lengths; therefore the calculations of G_{ic} placed greater emphasis on the experiments with longer embedded fibers.

Equation (7) is based on the actual specimen dimensions within the embedded fiber zone and not on the effectively-loaded matrix radius. In these experiments, the matrix droplet was

approximately hemispherical in shape with a droplet radius of R = 2.5 mm. By equating the volume of matrix from the point where the fiber enters the droplet to the end of the embedded fiber length to the equivalent cylinder of matrix, the effective matrix radius can be calculated to be

$$R_{eff} = \sqrt{l_e\left(R - \frac{l_e}{3}\right)} \tag{8}$$

This R_{eff} was used to calculate the V_m and V_f used in Eq. (7) and in the terms defined in the *Appendix*. Notice that once R_{eff} is determined that a value of G_{ic} can be calculated from each experimental point. There is no need to do any fitting or to determine the stress-transfer parameter β. By plotting G_{ic} results from each experimental result it is easy to recognize if it is a good material property that should be constant for a given polymer-fiber-sizing set of experiments.

4. RESULTS AND DISCUSSION

4.1. Strength calculations

By fitting experimental results for τ_d as a function of embedded fiber length, l_e, to Eq. (3), it was possible to determine τ_{ult} and β for each polymer-fiber-sizing set of experiments. The properties used to determine σ_T for these fits are given in Table 1. Some sample plots of the "best fits" for vinylester matrix with G3 sizing and three different fiber diameters are given in Fig. 2. All fits were excellent. From Eq. (3), it is apparent that τ_d approaches τ_{ult} as l_e approaches zero. Thus, the best-fit results for τ_{ult} correspond to the intercepts in plots like those in Fig. 2.

Table 2 lists all experimental results for τ_{ult} and β. For a given matrix and sizing, τ_{ult} was found to be independent of fiber diameter. Thus, τ_{ult} can be suggested as a good material property

for characterizing the fiber/matrix interface. We claim it is more realistic than the common practice of setting the interfacial shear strength to the value of τ_d determined from the peak load in the pull-out experiments. Using τ_{ult} as an interface characterization property, the interface strengths in the various fibers rank as PA6 ≥ PA66 > VE > PPM. For a constant polymer type, the sizings rank as G4 > G3 for VE matrix, G0 > G1 > G2 for PA6 matrix, and G1 > G0 ≥ G2 for PA66 matrix.

The measured β, however, was a function of fiber diameter — it was larger for specimens with smaller diameter fibers. The literature data on β variations with external conditions are rather scarce [9, 15, 24], and no information is available about the dependence of β on fiber radius. Elasticity models consider β to be a well-defined parameter whose value can be calculated from specimen geometry and elastic properties of the fiber and the matrix (see Eqs. (5) and (6)). Such calculations of β, however, depend on the effectively-loaded matrix radius, R_m. It has been shown experimentally that R_m can be considerably smaller than the specimen radius [15, 23]. Similar observations led to the "rule-of-thumb" proposed by Detassis *et al*. [19] that the R_m/r_f ratio in micromechanical tests should be taken in the region between 2 and 10, independent of the fiber radius and specimen size; but this assumption appeared to have only limited applicability. It was shown, in particular, that the β value for a given polymer-fiber system could be altered substantially as a result of fiber treatment [9, 24]. Furthermore, if the R_m/r_f ratio was a constant then β would be constant; our experiments demonstrated that R_m/r_f was neither constant nor "nominal" for fibers having different diameters.

A "physical" interpretation of β can be developed by considering its use in analyses of stress transfer. By experimental observations of fiber-matrix stress transfer (*e.g.*, by Raman spectroscopy [27]) or from elasticity models of stress transfer [25], the rate of stress transfer

between the fiber and matrix can always be described by an exponential function such that the extent of transfer is proportional to $\exp(-\beta z)$. Here z is the distance from any discontinuity such as a fiber break, a fiber end, or the point where the fiber enters the matrix in a pull-out test. For such a process, we can define:

$$t_{50} = \frac{\ln 2}{2r_f \beta} \tag{9}$$

The term t_{50} is the distance required, in dimensionless units of fiber diameters, for the stress transfer process to be 50% complete. Our results for t_{50} calculated from the measured β's are given in Table 2 and plotted in Fig. 3. The stress-transfer distance gets longer as the fiber radius gets smaller. This result is consistent with elasticity calculations of fiber/matrix stress transfer. Both numerical and shear-lag calculations for concentric fiber/matrix cylinders show that the stress transfer distance gets longer as the fiber volume fraction gets smaller [25]. For real specimens, this volume fraction should refer to an effective volume fraction calculated from the effectively-loaded matrix radius. Without experiments, it is not possible to tell whether such an effective fiber volume fraction should decrease or remain the same as the fiber radius gets smaller, but it is physically unreasonable for it to increase. The experimental results in Fig. 3, show that for this range of fiber radii and this size of matrix droplet, that the stress transfer rate increases, which implies that the effective fiber volume fraction decreases, and the fiber radius decreases.

The specimen fiber volume fractions in our experiments calculated using Eq. (8) were always low ($0\% < V_f < 0.1\%$). Although shear-lag analysis does not work when the specimen volume fraction gets too low, both Eqs. (5) and (6) have interesting low V_f limits that can be compared to experiments. In fact, both have the same limiting result that can be cast as

$$\lim_{V_f \to 0} \frac{1}{\beta^2 r_f^2} = \frac{E_f}{2G_m}\left(\ln R_m - \ln r_f\right) \tag{10}$$

Interestingly, the only time the Cox β (Eq. (5)) and the Nayfeh β (Eq. (6)) agree is at very low volume fraction, which is a regime for which shear-lag analysis breaks down [25]. For all volume fractions at which shear-lag analysis works, the two β's are different; the Nayfeh β gives a good prediction of stress transfer rates while the Cox β is very inaccurate. If R_m is assumed to be independent of r_f, which may not be a good assumption, Eq. (10) predicts that a plot of $1/(\beta^2 r_f^2)$ as a function of $\ln r_f$ should be linear with a slope of $-E_f/(2G_m)$ while the intercept can be used to calculate R_m. Such a plot is given in Fig. 4 for all experimental results. The plot is roughly linear, but there is too much scatter and insufficient distribution of fiber radii to confirm a linear relation. The slope of the "best-fit" line was –78.1. The four matrices had different values of G_m (and perhaps should not have been on the same plot) giving a range of actual $-E_f/(2G_m)$ from –30.5 to –78.0. Considering the qualitative nature of the analysis, the actual ratio agrees well with the measured slope. From the intercept of the "best fit" line, the R_m, which was assumed to be constant, was 41.7 μm. Using this result, R_m/r_f varied from 0.95 to 8.8. This range is reasonable [19] but the lower limit is too low. It may not be correct to assume, as done in this interpretation, that R_m is independent of fiber diameter.

Another route to R_m is to calculate it from the measured values for β and the shear-lag equations in Eqs. (5) and (6). The results of deducing effective fiber volume fractions, the ratio R_m/r_f, and the effectively-loaded matrix radius R_m using either the Cox β or the Nayfeh β are given in Table 2. Consistent with the stress transfer results in Fig. 3, the effective fiber volume fraction decreased as the fiber radius decreased. The related ratio R_m/r_f increased as the fiber radius decreased. For large fiber diameters (>50 μm), R_m/r_f was in the range 3.4 to 13.8 which is

the range commonly assumed for micromechanical tests [19]. For smaller fiber diameters (<30 μm), R_m/r_f got much larger. For large fiber diameters (>50 μm), R_m was much smaller than the specimen dimensions. For smaller fiber diameters (<30 μm), R_m got larger and equaled or exceeded the specimen dimensions. All these comments refer to results deduced when using the Nayfeh result for β. It is mathematically possible to deduce the same parameters using the Cox β (see Table 2). Because the Cox β is inaccurate, such calculated dimensions cannot meaningfully be compared to specimen dimensions.

4.2. Energy calculations

The same experimental results that were analyzed in the previous section for τ_{ult} and β can be analyzed for critical energy release rate using Eq. (7). Typical pull-out experiments record debonding force and embedded fiber length. To use Eq. (7), one additionally needs to know the effective fiber volume fraction. This term was determined here using Eq. (8). Some sample results for vinylester matrix with G3 sizing and three different fiber diameters are given in Fig. 5. Because G_{ic} can be calculated from each experimental result, the results for all three fiber diameters could be plotted on the same plot. These results, and all other fracture mechanics results, had a characteristic shape. At very short embedded fiber length, the calculated G_{ic} was low, but it increased rapidly eventually reaching a plateau value. The results for short embedded fiber length were low either because Eq. (7) was inaccurate or because the embedded fiber end influenced the debond initiation. Either way, the analysis worked better when the embedded fiber end was not too close to the debonding zone [26]. For a given polymer-fiber-sizing set of experiments, we, therefore, calculated the G_{ic} to be the average of the G_{ic} values in the plateau region. For most specimens, the plateau region was for embedded fiber lengths longer than

100 μm. For some of the larger radius fibers, the plateau regions required embedded fiber lengths of 150 to 200 μm.

The G_{ic} results for all fiber-sizing-matrix systems are listed in Table 2. For the PPM and VE polymers, G_{ic} was nearly independent of fiber diameter. For PA6 and PA66 polymers, however, G_{ic} depended on fiber diameter; it got smaller as the fiber diameter got larger. Comparing the different matrices, the interfacial toughness ranked as PA6 > PA66 > VE > PPM. This ranking agrees with the ranking determined from τ_{ult} calculations. For a constant polymer type, the interfacial toughnesses for the sizings rank as G4 > G3 for VE matrix and G0 > G1 = G2 for PA6 matrix. These rankings are nearly the same as the τ_{ult} rankings with the one exception being that the τ_{ult} rankings placed G2 < G1 instead of G2=G1 for the PA6 matrix. Furthermore, the results for G3 and G4 sizings were also obtained for many other polymer-fiber systems [22]. The G_{ic} ranking for the PA66 polymer was ambiguous and different than the τ_{ult} rankings. For small fiber diameter, the interfacial toughnesses for PA66 ranked as G0 > G2 > G1; for larger fiber diameters, the interfacial toughnesses of these three sizings were indistinguishable.

4.3 Strength vs. energy calculations

When looking at a single set of experiments with a constant fiber diameter, G_{ic} appears to be an excellent material property characterizing debonding. For a given polymer-fiber-sizing system, it was always constant within the plateau region of sufficiently long embedded fibers. When comparing experiments with different fiber diameters, however, τ_{ult} may be a better material property; τ_{ult} was independent of fiber diameter while G_{ic} sometimes depended on fiber diameter. For ranking interfacial properties, either material property may be used and they usually gave the same results. If G_{ic} is used, however, it can only be used to compare results with similar fiber diameters. For PA66 polymer systems, only the τ_{ult} results gave a clear ranking. It is possible,

however, that the interfacial properties for the three sizings with PA66 polymer were too close to be clearly distinguished using pull-out experiments.

Most work on crack or debond growth assumes fracture mechanics or energy methods are more fundamental than strength-based methods. It was somewhat surprising, therefore, that the strength analysis for τ_{ult} gave results that were more independent of specimen geometry than the energy analysis for G_{ic}. A possible explanation is that all our experiments were for *initiation* of debonding. Most experimental work in fracture mechanics analyzes growth of existing crack instead of initiation of a new crack. It is mathematically possible to calculate the energy release rate for initiation of debonding, but from our experiments, it appears that the conditions to cause initiation are determined by local stress rather than the initial energy release rate. It would be interesting to monitor load as a function of debond length and see if the fracture mechanics methods then give the preferred approach for prediction of debond *propagation*.

It is important to emphasize that the preferred strength analysis here is not the same as the strength analyses typically used for pull-out tests. Most strength models are simple *average* shear stress models that calculate the *average* interfacial shear stress at the point of failure using Eq. (1). The strength analysis here is based on the *local* or *maximum* interfacial shear stress. It is more difficult to determine τ_{ult} than τ_d. If β is known for a given system, τ_{ult} can be determined from τ_d using Eq. (3). If β is not known, τ_{ult} can be determined from the two-parameter fitting process used here. An advantage of such an analysis is that it additionally leads to an experimental result for the physically-meaningful β. A possible disadvantage is that the analysis for τ_{ult} requires experimental determination of two parameters. Although the G_{ic} calculations gave results that depended on fiber diameter, one advantage of the energy methods was that these results could be determined without knowledge of β.

5. CONCLUSION

1) Both ultimate IFSS (τ_{ult}) and critical energy release rate (G_{ic}) are sensitive to fiber treatment and, thus, characterize the interfacial bond strength.
2) The maximum shear stress failure criterion (τ_{ult}) gives results that are more independent of specimen geometry for *initiation* of debonding than the critical energy release rate (G_{ic}) criterion. The situation may be different for analysis of *propagation* of debonding.
3) Analysis of debonding stress as a function of embedded fiber length can be used to deduce and effective shear-lag parameter, β, which is a measure of the efficiency of load transfer from the fiber to the matrix. Both the dimensionless βr_f and the related R_m/r_f ratio are strong functions of the fiber radius.
4) The single-fiber pull-out test is a useful test for characterizing interfacial properties, but the data reduction must be done with care. Traditional *average* shear stress models are probably too simplistic. Such analyses should be replaced by *maximum* shear stress models or fracture mechanics models.

Appendix

The constants required for the fracture mechanics analysis of the pull-out test are defined by [26]:

$$C_{33s} = \frac{1}{2}\left(\frac{1}{E_A} + \frac{V_f}{V_m E_m}\right) \tag{A-1}$$

$$C_{33} = C_{33s} - \frac{V_m A_3^2}{V_f A_0} \tag{A-2}$$

$$D_{3s} = \frac{1}{2}(\alpha_A - \alpha_m) \tag{A-3}$$

$$D_3 = D_{3s} - \frac{V_m A_3}{V_f A_0}(\alpha_T - \alpha_m) \tag{A-4}$$

$$V_f A_0 = \frac{V_m(1-\nu_T)}{E_T} + \frac{V_f(1-\nu_m)}{E_m} + \frac{1+\nu_m}{E_m} \tag{A-5}$$

$$A_3 = -\left(\frac{\nu_A}{E_A} + \frac{V_f \nu_m}{V_m E_m}\right). \tag{A-6}$$

The new terms not previously defined in the paper are the transverse thermal expansion coefficient of the fiber (α_T), the transverse modulus of the fiber (E_T), the axial and transverse Poisson ratios of the fiber (ν_A and ν_T), and the Poisson ratio of the matrix (ν_m).

Acknowledgements

S. Zhandarov, E. Pisanova, and E. Mäder acknowledge the financial support from the European Community (project no. BETN 96 0507, Contract no. BRRT-CT97-5004). J. A. Nairn was supported by a grant from the Mechanics and Materials Program at the US National Science Foundation (CMS-9713356).

REFERENCES

1. M. J. Pitkethly, in: Fiber, Matrix, and Interface Properties, C. J. Spragg and L. T. Drzal (Eds.), ASTM STP 1290, pp. 34–46. ASTM, Philadelphia (1996).
2. I. Verpoest, M. Desaeger and R. Keunings, in Controlled Interfaces in Composite Materials, H. Ishida (Ed.), pp. 653–666. Elsevier, New York (1990).
3. M. R. Piggott, Composites Sci. Technol. 57, 965–974 (1997).
4. M. J. Pitkethly, J. P. Favre, U. Gaur, J. Jakubowski, S. F. Mudrich, D. L. Caldwell, L. T. Drzal, M. Nardin, H. D. Wagner, L. DiLandro, A. Hampe, J. P. Armistead, M. Desaeger and I. Verpoest, Composites Sci. Technol. 48, 205–214 (1993).
5. Yu. A. Gorbatkina, Adhesive Strength of Fibre–Polymer Systems. Ellis Horwood, New York (1992).
6. G. Désarmot and J.-P. Favre, Composites Sci. Technol. 42, 151 (1997).
7. M. J. Pitkethly and J. B. Doble, in Controlled Interfaces in Composite Materials, H. Ishida (Ed.), pp. 809–818. Elsevier, New York (1990).
8. S. F. Zhandarov and E. V. Pisanova, Composites Sci. Technol. 57, 957–964 (1997).
9. N. Takeda, D. Y. Song, K. Nakata and T. Shioya, Composite Interfaces 2, 143–155 (1994).
10. R. J. Scheer and J. A. Nairn, J. Adhesion 53, 45 (1995).
11. C.-H. Liu and J. A. Nairn, Int. J. Adhesion and Adhesives 19, 59–70 (1999).
12. M. R. Piggott, Carbon 27, 657 (1989).
13. H. L. Cox, Br. J. Appl. Phys. 3, 72 (1952).
14. A. H. Nayfeh, Fibre Sci. Technol. 10, 195–209 (1977).
15. M. Shioya, E. Mikami and T. Kikutani, Composite Interfaces 4, 429–445 (1997).

16. A. S. Nielsen and R. Pyrz, in ICCM-12: 12th Int. Conf. on Composite Mater. Paris, France, 5th-9th July 1999. Extended Abstracts, p.224. Paris, 1999.

17. M. C. Andrews, R. J. Young and J. Mahy, Composite Interfaces 2, 433–456 (1994).

18. C. Galiotis, Composites Sci. Technol. 42, 125 (1991).

19. M. Detassis, E. Frydman, D. Vrieling, X.-F. Zhou, H. D. Wagner and J. A. Nairn, Composites Part A 27A, 769–773 (1996).

20. E. Mäder, K. Grundke, H.-J. Jacobasch and G. Wachinger, Composites 25, 739–744 (1994).

21. L. B. Greszczuk, in Interfaces in Composites, ASTM STP 452, pp. 42–58. ASTM, Philadelphia (1969).

22. S. Zhandarov, E. Pisanova and B. Lauke, Composite Interfaces 5, 387–404 (1998).

23. S. Zhandarov, E. Pisanova and E. Mäder, Composite Interfaces, submitted (2000).

24. E. Pisanova and E. Mäder, J. Adhesion Sci. Technol. 14, 415–436 (2000).

25. J. A. Nairn, Mech. Materials 26, 63–80 (1997).

26. J. A. Nairn, Advanced Composite Letters, submitted (2000).

27. R. J. Young and M. C. Andrews, Mater. Sci. Engng A184, 197–205 (1994).

Table 1. Mechanical and thermal properties of the fiber and matrices used in this study

Property	E-glass	Modified polypropylene (PPM)	Vinylester resin (VE)	Polyamide 6 (PA6)	Polyamide 6,6 (PA66)
Tensile modulus (E_f or E_m) (GPa)	75	1.3	2.5	2.8	3.2
Poisson's ratio (ν_f or ν_m)	0.17	0.35	0.34	0.38	0.30
Shear modulus (G_f or G_m) (GPa)	32	0.48	0.93	1.01	1.23
Axial CTE (α_f orα_m) (ppm/°C)	5	150	65	65	81
Transverse CTE (α_T) (ppm/°C)	5	150	65	65	81
Stress-free temperature (°C)	—	<25	70	76	78

Table 2. Load transfer characteristics and interfacial parameters for polymer/glass fiber systems

Matrix	Fiber treat-ment	Fiber dia-meter (μm)	No. of points	β (mm^{-1})	t_{50} (Fib. diams)	Fiber strain at crack initiation	Ultimate IFSS (MPa)	Critical energy release rate (J/m^2)	Using Cox β			Using Nayfeh β		
									V_1	R_m/r_f	R_m (μm)	V_1	R_m/r_f	R_m (μm)
PPM	G1	12	18	18.5	3.12	0.0048	24.5	5.9	0.124	2.84	17.0	0.012	9.2	55.2
	G1	70...76	14	7.1	1.34	0.0015	21.2	7.1	0.703	1.19	43.4	0.058	13.8	500
VE	G3	11	11	12.3	5.12	0.0076	32.9	16.7	2.1×10^{-5}	220	1210	7.6×10^{-6}	360	1980
	G3	50...60	12	7.6	1.66	0.0019	37.9	14.7	0.322	1.76	48.4	0.0382	5.1	140
	G3	85...90	10	6.3	1.26	0.0011	34.5	13.0	0.524	1.38	60.4	0.0663	3.9	170
VE	G4	9...10	17	14.4	5.07	0.0120	42.7	25.3	1.6×10^{-6}	780	3700	6.1×10^{-7}	1280	6100
	G4	20...23	16	7.9	4.08	0.0077	42.9	34.0	0.0010	31	330	0.004	53	570
PA6	G0	12	12	12.8	4.51	0.0198	84.9	93.3	0.0001	97	580	3.9×10^{-5}	160	960
	G0	68	9	8.3	1.23	0.0035	79.8	40.1	0.507	1.40	47.6	0.0679	3.8	130
	G1	12	15	16.5	3.50	0.0135	76.1	49.9	0.0041	15.7	94	0.0013	28	170
	G1	76	9	8.7	1.05	0.0028	77.3	32.2	0.611	1.28	48.6	0.0890	3.4	130
	G2	14	17	11.7	4.23	0.0130	63.1	53.1	0.0003	56	390	0.0001	93	650
	G2	56	8	8.7	1.42	0.0029	59.5	24.8	0.404	1.57	44.0	0.0518	4.4	123
PA66	G0	12	12	12.6	4.58	0.0131	60.9	51.4	1.0×10^{-5}	320	1920	3.7×10^{-6}	520	3100
	G0	84	12	8.2	1.01	0.0011	56.0	23.8	0.576	1.32	55.4	0.0879	3.4	163
	G1	12	18	18.0	3.21	0.0102	70.73	35.2	0.0036	16.7	100	0.0012	29	174
	G1	65	13	9.1	1.17	0.0022	67.5	29.3	0.472	1.46	47.5	0.0671	3.9	127
	G2	14	19	11.8	4.20	0.0109	57.7	44.6	6.8×10^{-5}	120	840	2.5×10^{-5}	200	1400
	G2	62	10	8.4	1.33	0.0017	52.3	23.8	0.384	1.61	49.9	0.0529	4.4	136

V_1 is the effective fiber volume fraction, R_m is the effectively-loaded matrix radius, r_f is the actual fiber radius.

FIGURE CAPTIONS

Fig. 1. Typical force-displacement curve from a pull-out test. The debonding was assumed to initiate at the debond force, F_d, which corresponds to the knee in the force-displacement curve. F_d was always smaller than the maximum force value recorded during the test.

Fig. 2. Debond shear stress (τ_d) as a function of embedded fiber length for glass fibers with G3 sizing embedded in vinylester resin. The solid line is the best fit to Eq. (3). The fiber diameters were 11 μm (a), 50–60 μm (b) and 85–90 μm (c).

Fig. 3. The distance required for the stress transfer process to be 50% complete (in dimensionless units of fiber diameters from Eq. (9)) *vs* the fiber radius (for all experimental results).

Fig. 4. Experimental results for the dimensionless term $(\beta r_f)^{-2}$ as a function of ln r_f (when r_f is in μm). For details see text.

Fig. 5. Typical plot of the critical energy release rate (G_{ic}) as a function of the embedded length for glass fibers with G3 sizing embedded in vinylester resin. G_{ic} was calculated using the long-fiber analysis in Eq. (7).

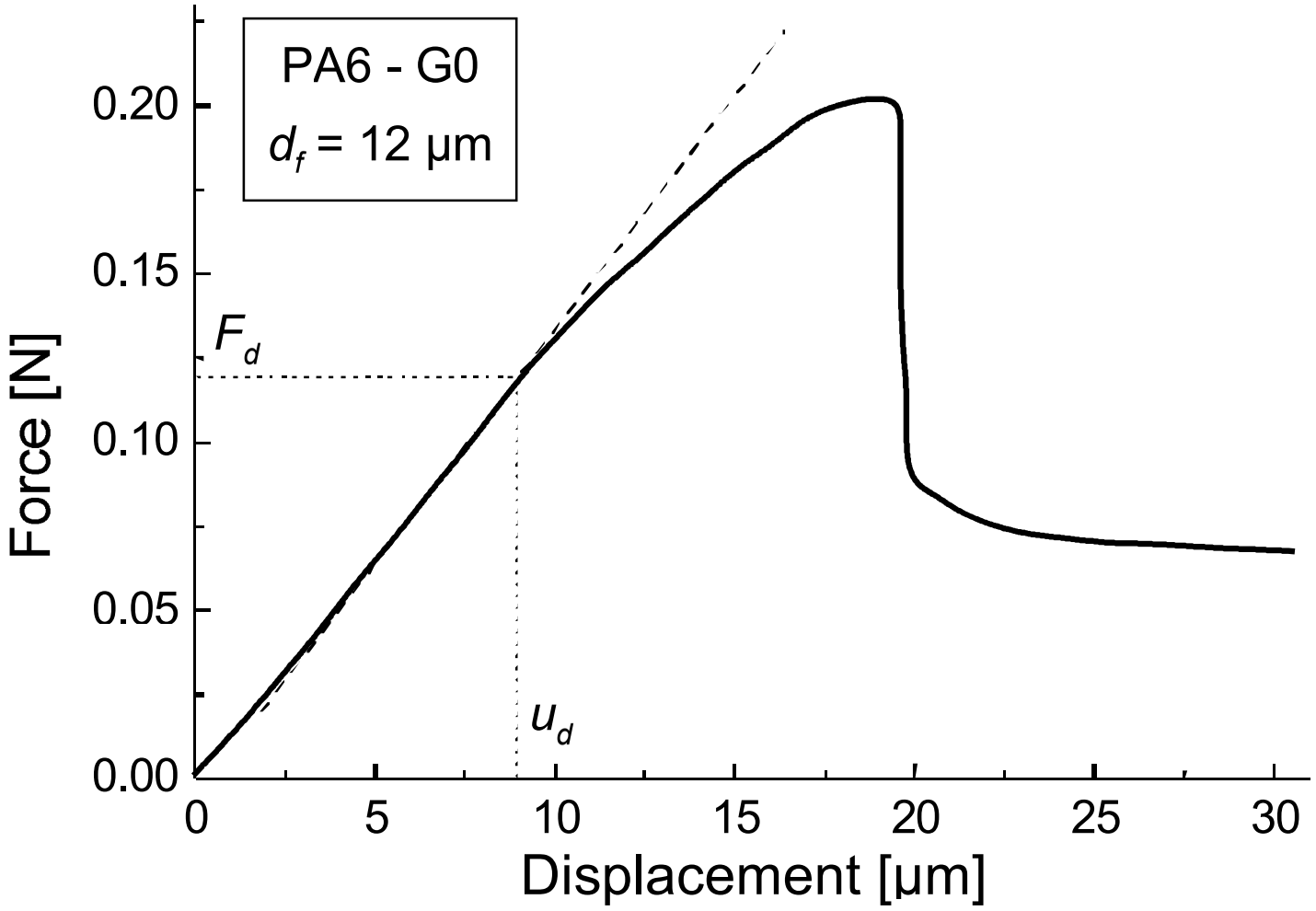

Zhandarov, Pisanova, Mäder, and Nairn
Fig. 1

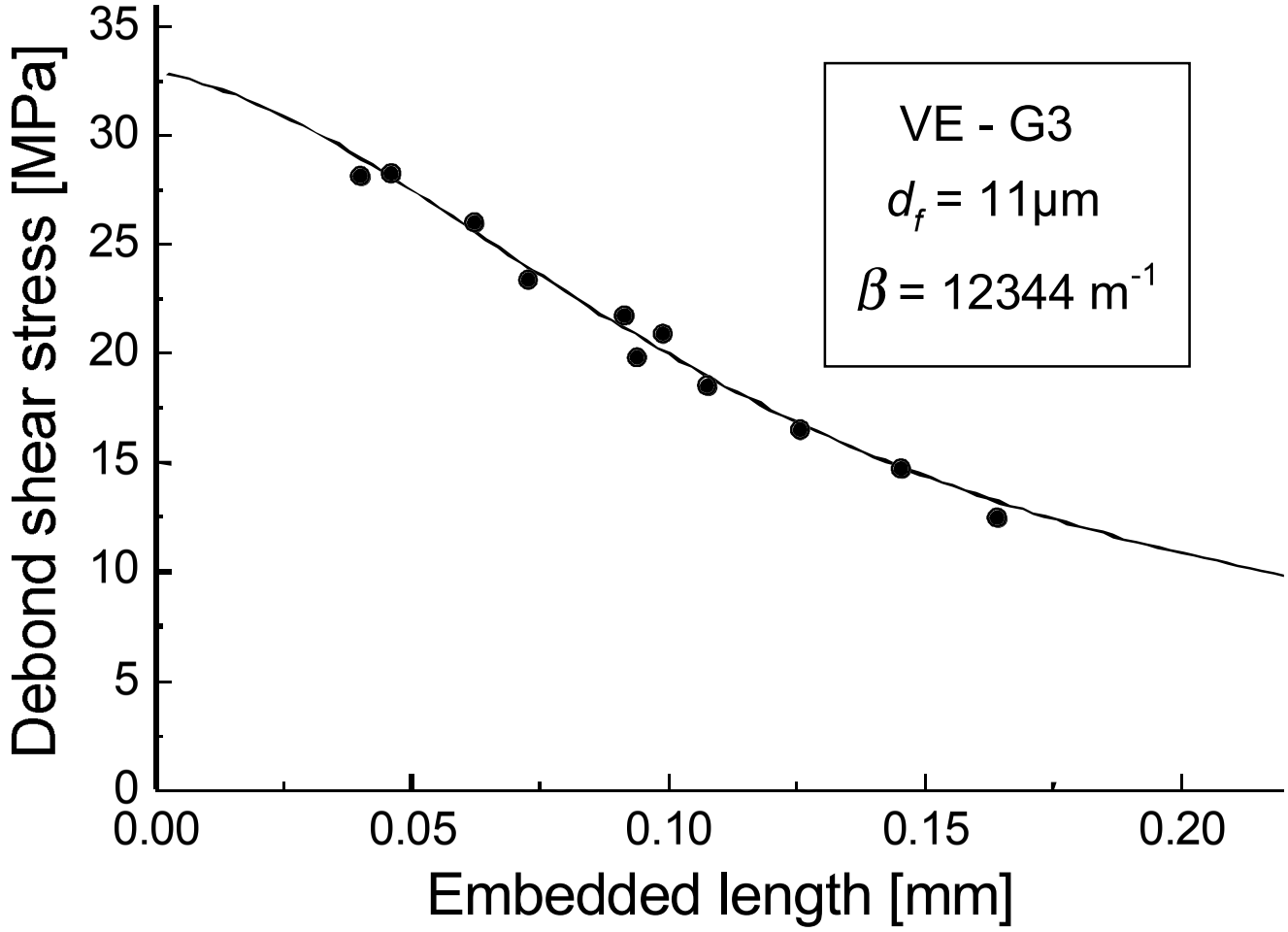

Zhandarov, Pisanova, Mäder, and Nairn
Fig. 2A

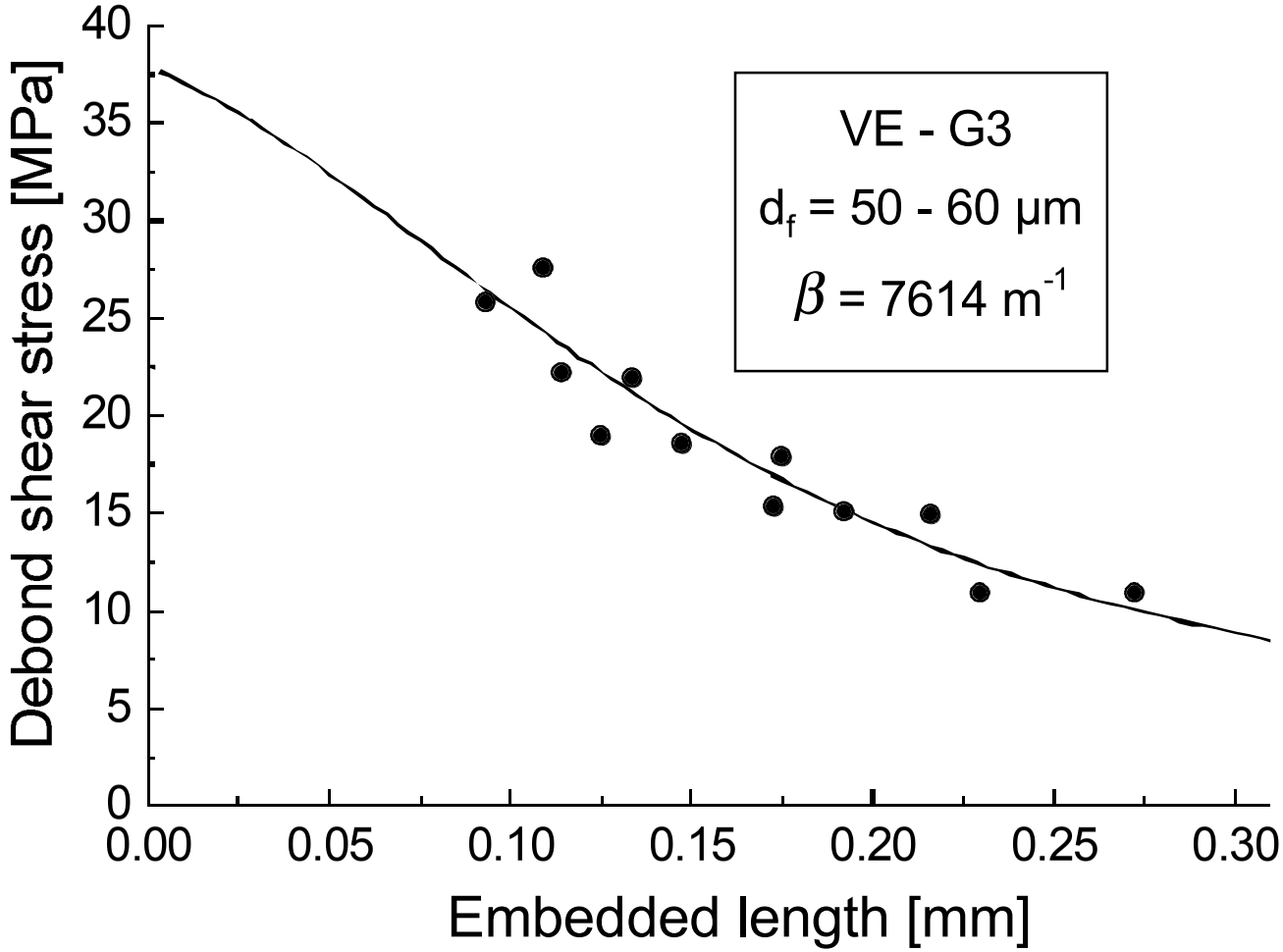

Zhandarov, Pisanova, Mäder, and Nairn
Fig. 2B

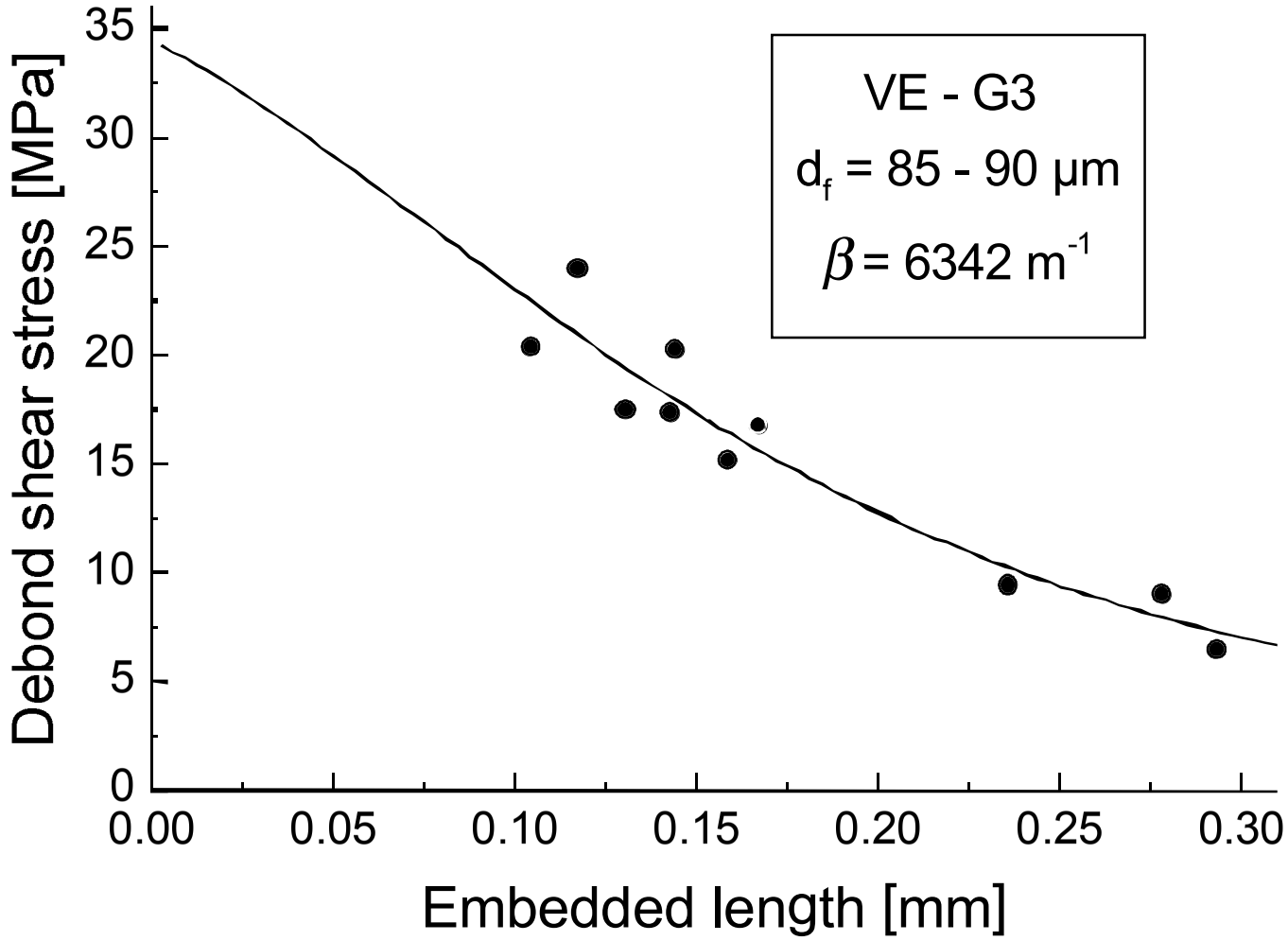

Zhandarov, Pisanova, Mäder, and Nairn
Fig. 2C

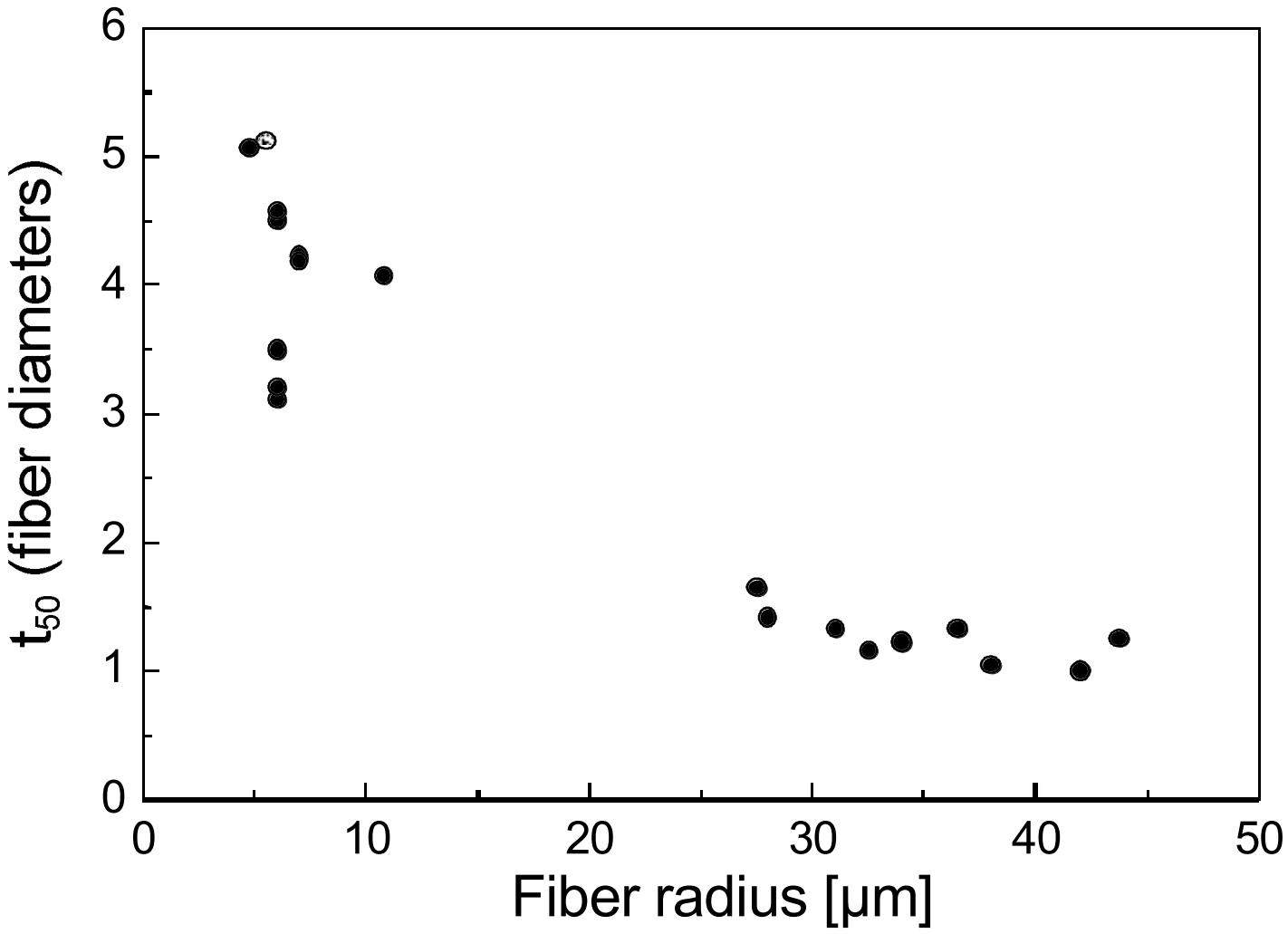

Zhandarov, Pisanova, Mäder, and Nairn
Fig. 3

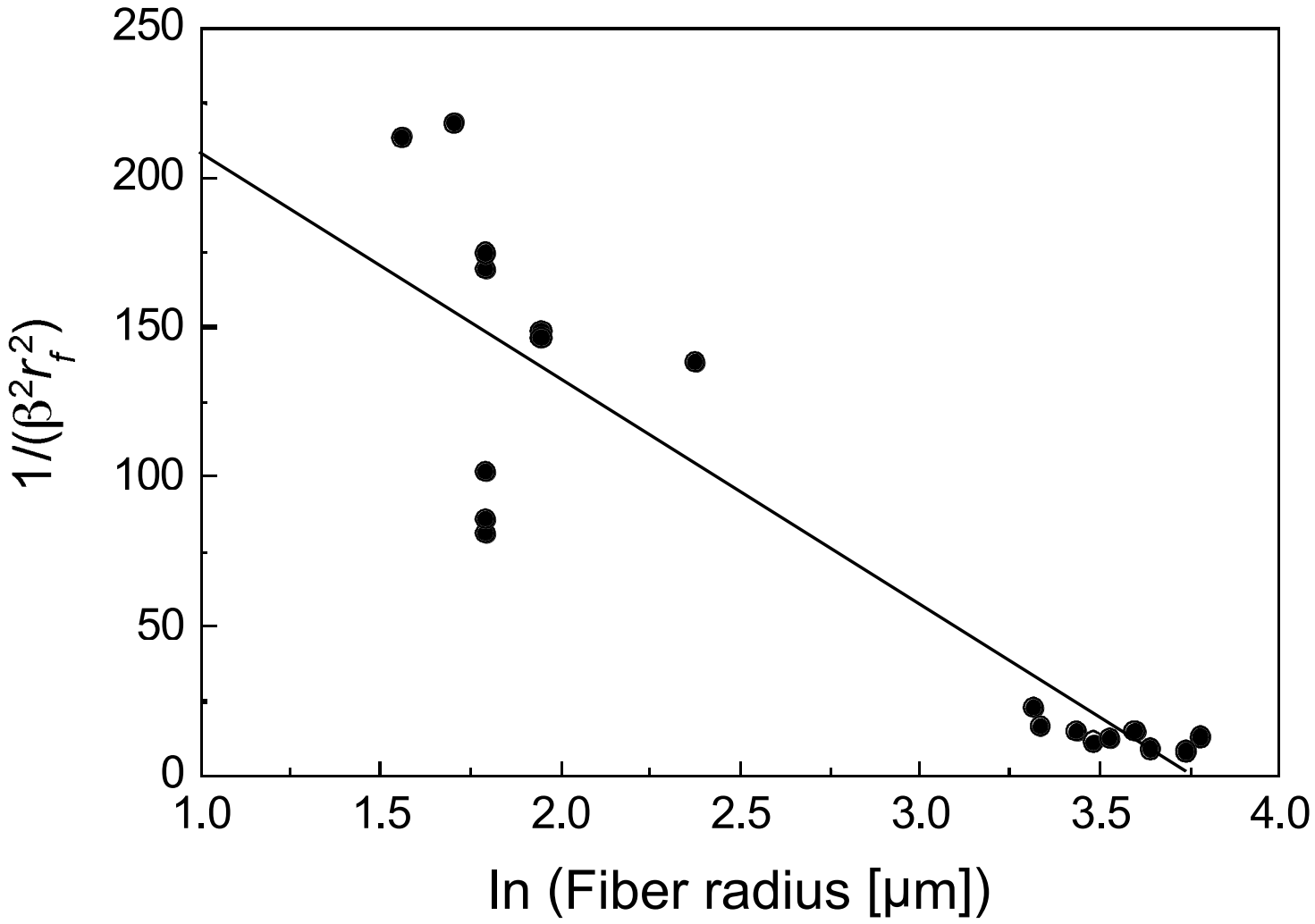

Zhandarov, Pisanova, Mäder, and Nairn
Fig. 4

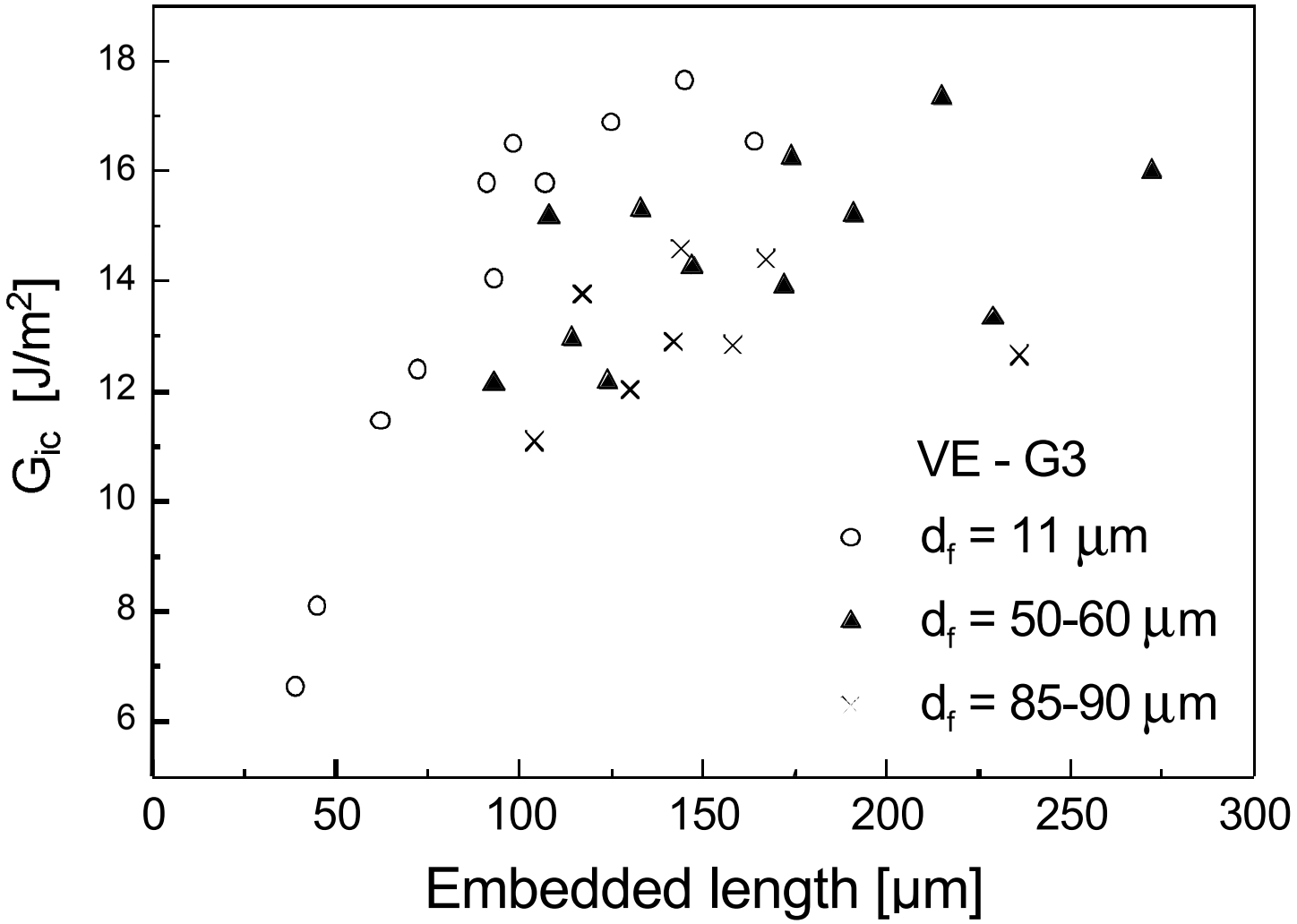

Zhandarov, Pisanova, Mäder, and Nairn
Fig. 5